ACS Sustainable Chemistry & Engineering

Research Article

pubs.acs.org/journal/ascecg

Optical and Photocatalytic Properties of Solar Light Active Nd-Substituted Ni Ferrite Catalysts: For Environmental Protection

K. N. Harish, H. S. Bhojya Naik,* P. N. Prashanth kumar, and R. Viswanath

Department of Studies and Research in Industrial Chemistry, School of Chemical Sciences, Kuvempu University, Shankaraghatta-577 451, India

ABSTRACT: In the present investigation, we have reported the fabrication of a low-cost, magnetically separable, solar light active $NiFe_{2-x}Nd_xO_4$ photocatalyst with different neodymium contents. The synthesized photocatalyst samples were characterized by a combination of various physicochemical techniques such as PXRD, SEM, EDS, FTIR, and UV−vis spectroscopy. It was observed that Nd substitution can greatly enhance absorption in the whole visible region. With an increase in Nd concentration, $NiFe_{2-x}Nd_xO_4$ samples show a red shift in absorption. Interestingly, Nd substitution into nickel ferrite results in a dramatic conversion of the inert $NiFe_2O_4$ into a highly solar light active photocatalyst for the degradation of organic pollutants and also shows excellent recyclability and durability properties. The significant enhancement in photoactivity under solar light irradiation can be ascribed to the reduction of the nickel ferrite band gap by Nd^{3+} substitution. Therefore, these unusual properties of $NiFe_{2-x}Nd_xO_4$ encourage us to extend photocatalytic degradation to another few organic pollutants. This new photocatalyst system, $NiFe_{2-x}Nd_xO_4$, can have other potential environmental and energy applications that only need visible light as energy input.

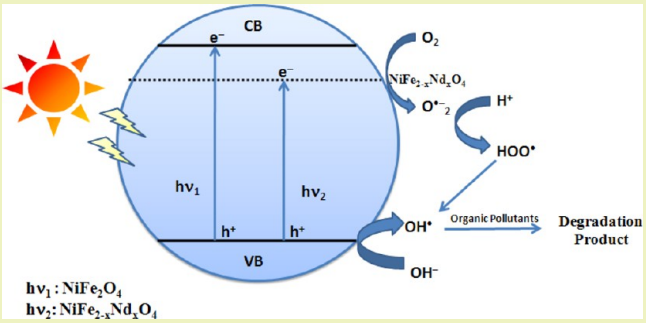

KEYWORDS: *Solar energy, Magnetic separation, Photocatalysts, Optical properties*

INTRODUCTION

Catalysis is becoming a strategic field of science because it represents a new way to meet the challenges of energy and sustainability. These challenges are becoming the main concerns of the global vision of societal challenges, world economy, and environmental safety. Environmental contaminants in water or air pose a serious threat to public health and safety. They have attracted considerable attention from a range of research groups. More than 7×10^5 tons of synthetic dyes are produced every year worldwide. About 10−15% of these dyes are lost as waste pollutants entering into the environment.[1] Synthetic dyes usually contain complex aromatic structures that are chemically stable and resistant to biodegradation in nature. Their toxicity and persistence in the environment are of a great concern to aquatic life and human health.[2,3] Treatment and cleaning of these pollutants from wastewater thus becomes an essential issue of environmental and health protection. Because of the large degree of organics present in wastewater and the stability of modern textile dyes, conventional biological treatment methods are ineffective for their decolorization and degradation of wastewater.[4] Consequently, novel technologies with more efficiency and less energy use have stimulated intensive research. An alternative to the conventional method is photocatalytic degradation, i.e., advanced oxidation processes based on the generation of very reactive species such as hydroxyl radicals (•OH) that oxidize a broad range of organic pollutants quickly and nonselectively.[5]

The consumption of nonrenewable energy sources such as fossil fuels for photodegradation is less favorable nowadays, not only because of current shortage and a final exhaustion of these sources but also for serious environmental considerations.[6,7] The vast clean energy source that remains incompletely exploited is solar energy. With an annual insolation level of 1000 W/m^2, solar energy is an attractive energy source that exceeds all current human needs.[3,4] The conversion of solar energy (electromagnetic radiation) into a practically applicable form can be achieved by a photocatalyst (i.e., semiconductor with an appropriate band gap and band edges) through a process that is similar to photosynthesis.[7−11]

In recent years, semiconductor photocatalysis, as a "green" technology, has been widely used for the treatment of polluted water. Most of them suffer from their intrinsic limitations (band gap > 3.1 eV) that only ultraviolet radiation can be utilized.[12,13] However, it is well known that although the sun can provide an abundant source of photons, UV light accounts for only a small fraction (4%) of the solar energy compared with visible light (45%), indicating that low band gap catalysts are more desirable. In this respect, developing a photocatalyst that efficiently extends photocatalytic activity into visible region for environmental remediation has become a great challenge and

Received: March 2, 2013
Revised: June 5, 2013
Published: June 28, 2013

one of the most active research topics in photocatalysis.[14−16] Usually, photodegradation reactions are carried out in heterogeneous systems. The ability to reuse the suspended ultrafine photocatalysts after degradation can result in substantial cost savings. The introduction of magnetic nanoparticles to a variety of solid matrixes allows the combination of well-known procedures for photocatalyst heterogenization with techniques for magnetic separation.[17]

Use of ecofriendly ferrites[18−21] for efficient solar energy usage has been an important topic in visible light photocatalysis research. Ferrites are well known for their tremendous applications in the field of magnetic and electronic materials,[22,23] but there are few reports on their photocatalyst applications.[24,25] Unlike TiO_2, ferrites offer an advantage of displaying a desirable optical absorption for low energy photons ($h\nu \sim 2$ eV) and of exhibiting the well-suited electronic structure desirable for photocatalytic applications. To make full use of solar energy, many attempts have been made to prepare the narrow band gap ferrite semiconducting material that utilizes the much larger visible region. Some of the recent reports are important indicators with respect to the potential of visible light photocatalytic application of spinel ferrites.[25−27] Among the ferrites, owing to unique properties of low price, environmental benignity, and the large abundance of Ni, $NiFe_2O_4$ has received great attention and is one of the most important magnetic materials with high electrical resistivity, high Curie temperature, and environmental stability. As an important class of magnetic materials, $NiFe_2O_4$ with an inverse spinel structure has ferrimagnetism that originates from a magnetic moment of antiparrallel spins between Fe^{3+} ions at tetrahedral sites and Ni^{2+} ions at octahedral sites.[28] The properties of nickel ferrite can be varied by changing the identity of the trivalent Fe^{3+} and divalent M^{2+} cations. Even though, $NiFe_2O_4$ has a band gap of 2.19 eV,[29] little research has been conducted on its photocatalytic activity. Although $NiFe_2O_4$ alone is photocatalytically inactive under visible light irradiation,[30] it is possible to improve the efficiency of the photoinduced charge separation in $NiFe_2O_4$ by substituting metals, resulting in enhanced photocatalytic performance. It has been reported that Kundu et al.[31] investigated the microstructure and dc resistivity of Ti^{4+} ion-doped nickel ferrites. Peng et al.[32] studied the effect of Pr^{3+} doping on magnetic and dielectric properties of Ni−Zn ferrites. Xu et al.[33] reported the photocatalytic properties of magnetically separable TiO_2 supported on nickel ferrite. Singh et al.[34] demonstrated the multiferroism in gadolinium-substituted nickel ferrite. Ishaque, et al.[35] investigated the electrical and dielectric properties of yttrium-substituted nickel ferrites. To the best of our knowledge, as per the literature, no reports have been cited on the photocatalytic properties of magnetically recoverable neodymium-substituted nickel ferrite nanoparticles under solar light irradiation to date.

It is of great interest to explore a novel approach for imparting multifunctional properties onto the neodymium-substituted nickel ferrite system. If that can be accomplished, then it may be possible to obtain widely useful material with good recycling stability and also have high performance under solar light irradiation as well as with a great magnetic recycling property (as photocatalysts). In our previous work, we have shown that visible light activities of $ZnFe_2O_4$ photocatalysts could be markedly improved by substitution with a cadmium metal.[36] This work actually motivated us with further interest to design solar light driven ferrite photocatalysts substituted with different metals. Herein, we report the synthesis of a neodymium-substituted nickel ferrite system by a modified size-controlled coprecipitation method. Interestingly, when neodymium is substituted into nickel ferrite, the inactive $NiFe_2O_4$ dramatically converted into a solar active photocatalyst. The photocatalytic activity of the pure and neodymium-substituted nickel ferrite under natural solar light was investigated and reported for the first time.

EXPERIMENTAL SECTION

Preparation of Catalysts. Nanocrystalline neodymium-substituted nickel ferrite nanoparticles were synthesized by the chemical coprecipitation method.[37] The starting materials are of high-purity $Fe(NO)_3{\cdot}9H_2O$, $Ni(NO_3)_2{\cdot}6H_2O$, and $NdCl_3{\cdot}6H_2O$. According to the formula of $NiFe_{2-x}Nd_xO_4$ (where x = 0.0, 1.0, 1.5 2.0), each starting material was weighed and dissolved in double distilled deionized water and then mixed together. Sodium hydroxide (GR, 28−30%) of 3.0 M (as the precipitating agent) was added to the salt solution dropwise. The pH of the solution was constantly monitored as the NaOH solution was added dropwise. The reactants were constantly stirred using a magnetic stirrer until a pH level of 13 was achieved. A specified amount of oleic acid (2−3 drops for total reacting solution of 75 mL) was added to the solution as the surfactant. The liquid precipitate was then brought to a reaction temperature of 80 °C and stirred for 60 min. The product was cooled to room temperature and then washed twice with double distilled water and ethanol to remove unwanted impurities and the excess surfactant from the prepared sample. The size and size distribution was controlled by controlling the nucleation and growth rates during the reaction. Smaller particles were obtained if the nucleation rate was higher than the growth rate. Large pH values (above12) were used because they control the process of nucleation (rate) and lower the particle sizes.[38] Nd-concentration(x) in nickel ferrite has been controlled by the initial stoichiometric ratios of the reactants.

Characterization. Physical and chemical characterizations of $NiFe_{2-x}Nd_xO_4$ were carried out as described below. Light absorption properties of the $NiFe_{2-x}Nd_xO_4$ nanocrystals dispersed in ethanol were studied by a UV−vis spectrophotometer (Shimadzu, UV-1650 PL model). The phase compositions and structures of the $NiFe_{2-x}Nd_xO_4$ samples were determined by powder X-ray diffraction (PXRD, PANalytical Xpert Pro X-ray diffractometer) with Cu Kα radiation (k = 0.15406 nm) over the 2θ range of 10−80°. The structural characterization of the nanocrystalline $NiFe_{2-x}Nd_xO_4$ samples were examined by Fourier transform infrared spectroscopy (FTIR) (using a Nicolet IR200 FT-IR spectrometer). The morphology of $NiFe_{2-x}Nd_xO_4$ ferrite samples was observed by scanning electronic microscopy (SEM) with a JSM-6700 LV electron microscope operating at 5.0 kV, and the chemical compositions were examined by energy dispersive X-ray spectroscopy (EDS).

Photocatalytic Activity Study. The reactions of the photocatalytic degradation of organic pollutants with synthesized $NiFe_{2-x}Nd_xO_4$ catalysts samples were measured under natural solar light irradiation in an aqueous solution at ambient temperature. Experiments conducted are as follows. In each experiment, 0.1g of $NiFe_{2-x}Nd_xO_4$ nanoparticles were added into 100 mL of rose bengal solution with a concentration of 10 mg L^{-1}. The suspension was magnetically stirred in the dark for 30 min to establish the adsorption/desorption equilibrium at room temperature, and then the solution was directly irradiated under natural solar light with similar conditions on sunny days of March−May between 10 a.m. and 3 p.m. where the solar intensity fluctuations were minimal. The sky was clear, and the sun's rays were very intense in this period in the city of Shivamogga (India). During irradiation, stirring was maintained to keep the mixture in suspension. At regular intervals, samples were taken from the suspension and then magnetically separated to remove $NiFe_{2-x}Nd_xO_4$ nanoparticle catalysts to be reused for additional runs. The color removal of the dye solution was monitored on a UV−vis spectrophotometer (Shimadzu, UV-1650 PL model) by measuring the absorbance in the range of 200−800 nm wavelength. Distilled

water was used as the reference sample. According to the calibration plot of the UV absorbance as a function of the remaining rose bengal concentration, the efficiency of the rose bengal decomposition was calculated. In addition, we investigated the recyclability of $NiFe_{2-x}Nd_xO_4$, and after each catalytic run, the sample was washed and dried to permit subsequent photoreaction cycles.

RESULTS AND DISCUSSION

Structure and Morphology of $NiFe_{2-x}Nd_xO_4$ Photocatalysts. The X-ray diffractograms of the $NiFe_{2-x}Nd_xO_4$ (x = 0, 1.0, 1.5, 2.0) system are presented in Figure 1.

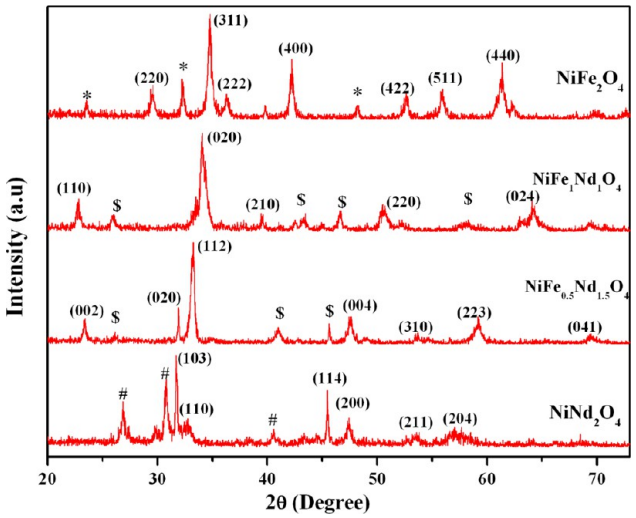

Figure 1. Comparative XRD patterns of $NiFe_{2-x}Nd_xO_4$ photocatalysts.

Experimentally observed d-spacing values, 2θ values, and relative intensities are in well agreement with the standard XRD pattern. When the ferrite is doped with a relative amount of rare earth ions, besides the spinel phase, a foreign phase in a small amount is formed.[39] Accordingly, $NiFe_2O_4$ (x = 0.0) particles exhibited the cubic phase with space group Fd3m (SG no. 227, JCPDS card no. 86-2267), and in addition, a peak designated by ∗ may be due to the formation of a small amount of α-Fe_2O_3 phase. As shown in Figure 1, the substitution of Fe^{3+} (r = 0.78 Å) by Nd^{3+} (r = 1.16 Å) determines a gradual change in the crystalline structure from a cubic to orthorhombic one. Thus, in the Nd-substituted ferrites ($NiFe_1Nd_1O_4$ and $NiFe_{0.5}Nd_{1.5}O_4$) the initial cubic phase of the nickel ferrite coexisted with the newly formed orthorhombic phase of $NdFeO_3$ (Figure 1, peak designated by $). The formation of the $NdFeO_3$ secondary phase can be explained by the limited solubility of voluminous Nd^{3+} ions in the host spinel lattice.[58] An oxide having a distorted tetragonal structure was obtained for a substitution of x = 2 ($NiNd_2O_4$), and in addition, a peak designated by # may be due to the formation of a small amount of Nd_2O_3 phase. In the $NiNd_2O_4$ structure, the Nd^{3+} and Ni^{2+} ions are surrounded by 8 and 4 O^{2-}, respectively.[40]

The XRD results were used to determine the average crystallite sizes of the $NiFe_{2-x}Nd_xO_4$ nanocrystals based on the FWHM values. The Debye−Scherrer formalism was applied (crystallite size = $0.89\lambda/\beta \cos\theta$, where λ = wavelength of X-ray, β = full width at half-maxima, and θ = diffraction angle), which results in an average crystal size of 22, 23, 24, and 19 nm with respect to x = 0.0, 1.0, 1.5, and 2.0. The value of the lattice constant for $NiFe_{2-x}Nd_xO_4$ was found to be a = 8.34, 8.78,

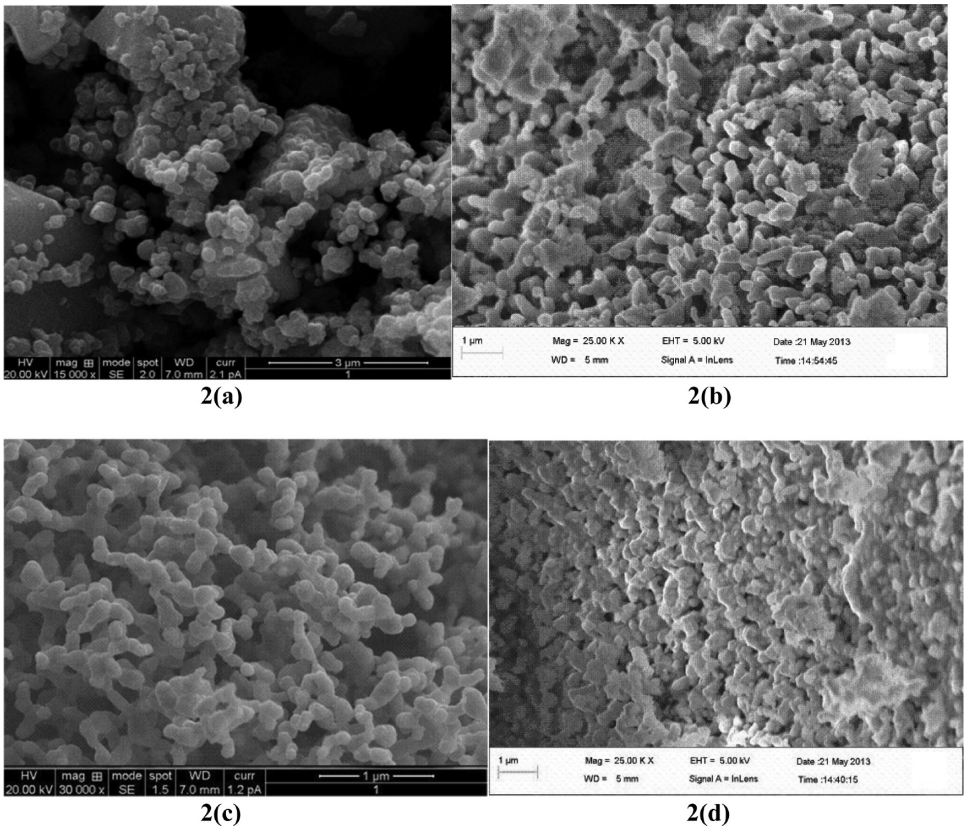

Figure 2. SEM micrographs of x = 0.0 (a), x = 1.0 (b), x = 1.5. (c), and x = 2.0 (d) samples.

dx.doi.org/10.1021/sc400060z | ACS Sustainable Chem. Eng. 2013, 1, 1143−1153

8.92, and 9.3 Å for the samples x = 0.0, 1.0, 1.5, and 2.0, respectively. It was observed that the lattice parameter increases linearly with Nd^{3+} concentration obeying Vegard's law. This can be explained on the basis of relative ionic radii of Fe^{3+} and Nd^{3+} ions. Because Fe^{3+} ions have smaller ionic radii (0.78 Å) than those of Nd^{3+} ions (1.16 Å), a partial replacement of the former by the later causes an increase in ionic radii on the B site. Shinde et al.[41] reported a similar behavior for Nd^{3+}-substituted nickel ferrites, and an increase in lattice constant with an increase in Nd^{3+} content in nickel ferrites is also reported by Vermenko et al.[42] The obtained value of the lattice parameter for nickel ferrite is in good agreement with the reported values.[43]

SEM and EDS Analysis. The SEM micrographs of the as-synthesized samples x = 0.0, 1.0, 1.5, and 2.0 are shown in Figure 2. The results illustrate that the morphology of the samples changes significantly with the change in the Nd concentration. Surface morphology of the sample at x = 1.5 shows a fine-structured morphology. However, the sample at x = 0.0 shows that some small particles get aggregated together to form bigger particles. The EDS spectra of synthesized photocatalysts illustrated in Figure 3(a,b) indicate that the

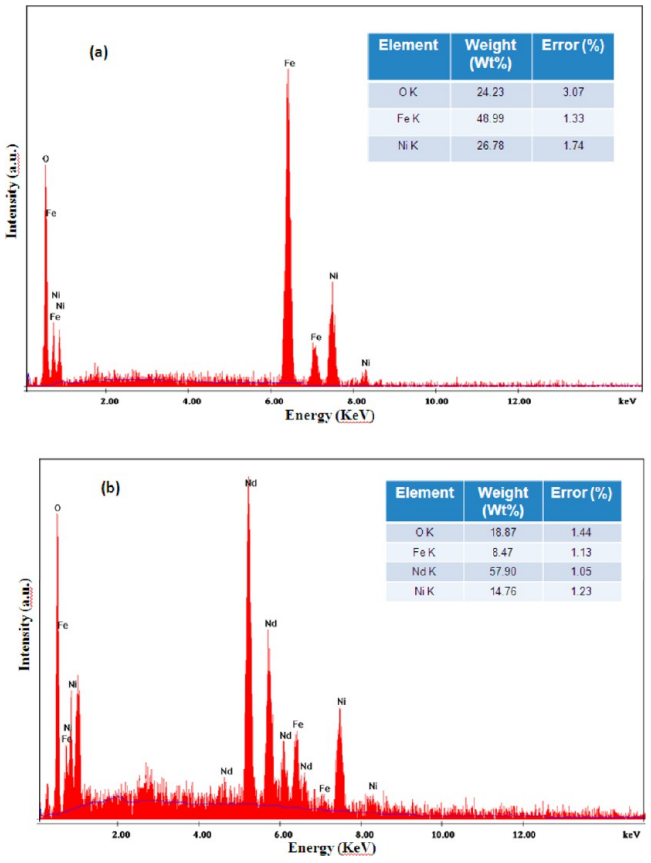

Figure 3. EDS spectra of x = 0.0 (a) and x = 1.5 (b) samples.

presence of Ni, Fe, Nd, and O atoms are the major chemical components present in the samples. The photocatalysts have a majority of 26.78 wt % of Ni, 48.99 wt % of Fe, and 24.23 wt % of O, for the sample x = 0.0 and 14.76 wt % of Ni, 8.47 wt % of Fe, 57.90 wt % of Nd, and 18.87 wt % of O, for the sample x = 1.5. The EDS results were consistent within experimental stoichiometric ratio with small experimental error, confirming the compositional uniformity and formation of the Ni-$Fe_{2-x}Nd_xO_4$ nanocatalysts synthesized by coprecipitation method. A large amount of Nd in sample x = 1.5 indicates the correct method of preparation and high photocatalytic efficiency. Meanwhile, a significant amount of Fe encourages the photocatalyst for better recovery with a strong magnetic property.

FTIR Analysis. The FTIR spectrum of $NiFe_{2-x}Nd_xO_4$ nanocatalysts is presented in Figure 4. In normal ferrites,

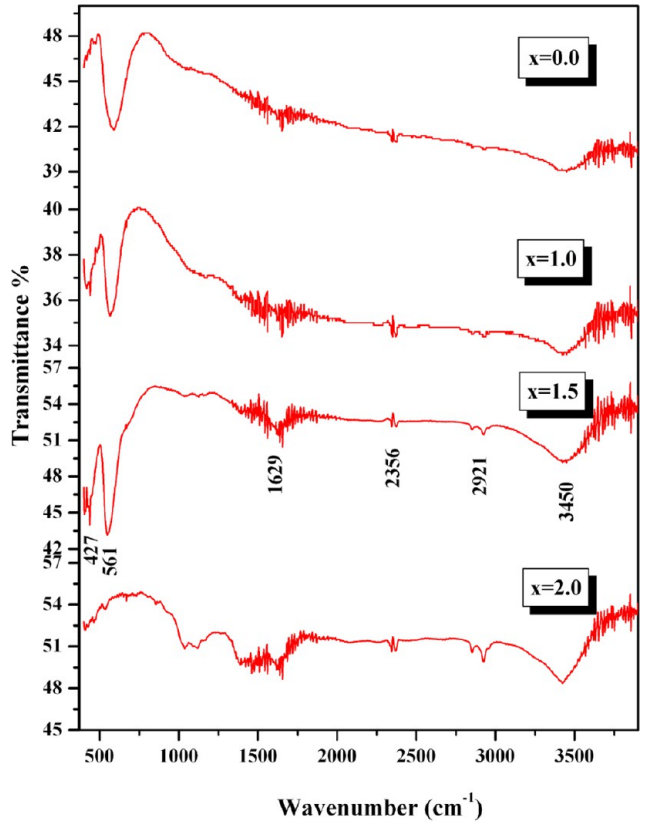

Figure 4. FTIR analysis of the $NiFe_{2-x}Nd_xO_4$ nanoparticles.

there are two high frequency infrared lattice vibrations. The bands, ν_1 and ν_2, are sensitive to changes in interaction between oxygen and cations in the octahedral and tetrahedral positions. The highest one, ν_1, is generally observed in the range of 600–500 cm^{-1} corresponding to intrinsic stretching vibrations of the metal at the tetrahedral site (T_d) $M_{tetra} \leftrightarrow O$ [A site], whereas the lowest band, ν_2, observed in the range 450–385 cm^{-1} is assigned to octahedral-metal stretching (O_h) $M_{octa} \leftrightarrow O$ [B site].[44] The absorption bands observed at ~3450 and ~1630 cm^{-1} prove the presence of adsorbed water on the surface of the ferrite nanocrystals. The bands occurring at ~2925–2854 cm^{-1} are assigned to antisymmetric and symmetric CH_2– vibrations of the carbon chains respectively. The positions corresponding to higher (ν_1) and lower (ν_2) frequency absorption bands of the samples prepared under investigation are given in Table 1. It was observed that the absorption band ν_2 shifts slightly to a higher wavenumber side and ν_1 shifts to a lower wavenumber side with an increase in Nd^{3+} content (up to x = 1.5). The shifts in the bands ν_1 and ν_2 are due to the perturbation occurring in the Fe^{3+}–O^{2-} bond by substituting Nd^{3+} ions, and also, it is attributed to an increase in bond length on the B site. This suggests that the Nd^{3+} ion occupies the B site. A similar type of variation in band positions is

dx.doi.org/10.1021/sc400060z | ACS Sustainable Chem. Eng. 2013, 1, 1143–1153

Table 1. Values of Absorption Bands (ν_1 and ν_2) for $NiFe_{2-x}Nd_xO_4$ Nanoparticles

	absorption band	
composition (x)	ν_1 (cm^{-1})	ν_2 (cm^{-1})
0.0	578	409
1.0	569	418
1.5	561	427

reported by Shinde et al.[41] for Nd^{3+}-substituted nickel ferrites. Hemeda et al.[45] discussed similar results for rare earth-substituted orthoferrites. From Figure 4, it is also observed that the width of absorption bands of Nd^{3+}-substituted nickel ferrites are smaller as compared to nickel ferrite, suggesting the occupancy of Nd^{3+} ions on the octahedral B sites. For the sample at x = 2.0, complete replacement of Fe^{3+} by a large amount of Nd^{3+} gives rise to a complete disappearance of the ν_1 and ν_2 bands, which assures the dominance of the Nd^{3+} in the nickel ferrite.[46]

Optical Absorption Studies. Optical absorption properties of photocatalysts are very important in the photocatalysis process. Figure 5 shows a comparison of the photon

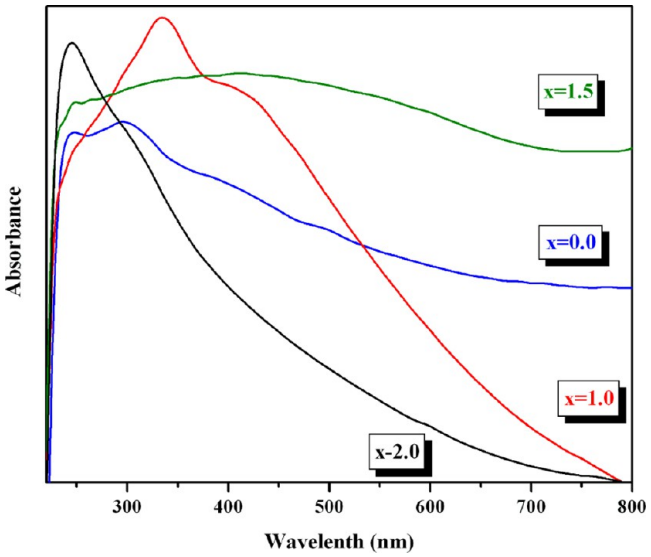

Figure 5. Optical absorption spectra of $NiFe_{2-x}Nd_xO_4$ samples.

absorbance of incident light as a function of the wavelength for the $NiFe_2O_4$ and Nd-substituted $NiFe_2O_4$ photocatalysts, which is helpful to distinguish theoretically whether the nanostructured composites are highly efficient photocatalysts or not. Figure 5 reveals that absorption edge is red shifted for Nd-substituted samples. As Nd content increases, the absorption edge shifted to a longer wavelength. The sample at x = 1.5 had the largest red shift and revealed a higher intensity overall visible light absorbance spectrum in comparison with other samples (x = 0.0, 1.0, and 2.0). This means that the Nd-substituted $NiFe_2O_4$ are sensitive to visible light. Enhanced visible light absorption may result from the following: $NiFe_2O_4$ is characterized by a inverse spinel structure in which the tetrahedral and octahedral sites within the lattice of cubic close packing are occupied by Ni^{2+} and Fe^{3+} cations,[47] and the energy band structures of $NiFe_2O_4$ are generally defined by considering the O-2p orbital as the valence band and the Fe-3d orbital as the conduction band. Therefore, the absorption of $NiFe_2O_4$ in the visible region can be ascribed to the photoexcited electron transition from the O-2p level into the Fe-3d level.[48] In $NiFe_2O_4$, the band gap between the O-2p level and the Fe-3d level is 2.29 eV, which is a large band gap compared to the neodymium-substituted samples. The band gap between the O-2p and Fe-3d level decreases to 1.96 and 1.76 eV with respect to x = 1.0 and 1.5 as shown in Figure 5. Because of the decrease in optical energy band gap (Eg), energy required to excite the electron from O-2p into the Fe-3d level goes on decreasing.[36] Along with the increasing Nd^{3+} concentration, the absorbance increases. The absorbance gradually increases with the increase in neodymium content up to x = 1.5. For the sample at x = 2.0, the absorbance decreases. The sample at x = 1.5 shows a quite broad absorption due to the charge−transfer transition between the Nd f-electrons and the $NiFe_2O_4$ conduction or valence band.[49] It has been reported that Nd doping could form a dopant energy level within the band gap of $NiFe_2O_4$. The electronic transitions from the valence band to the dopant level or from the dopant level to the conduction band can effectively lower the electron−hole pair recombination rate, which shifts the broad absorption band toward the visible region. Meanwhile, the sample at x = 0.2 shows blue shift of absorption in comparison with other samples. Because octahedral Fe^{3+} cations are completely replaced by the Nd^{3+} ions, the dopant energy levels are not formed within the energy gap. This leads to the faster recombination of electron−hole pairs, which is unfavorable for the photocatalytic reaction. Therefore, optimized Nd-substituted nickel ferrite makes it possible to utilize a higher percentage of solar energy. So for the $NiFe_{2-x}Nd_xO_4$ samples, a better photocatalytic capability under solar light was expected.

Energy Band Gap Studies. The optical energy band gap (Eg) of $NiFe_{2-x}Nd_xO_4$ catalysts were determined from the absorbance spectra, where a steep increase in the absorption is observed due to the band−band transition using the general relation. The absorption coefficient α of the $NiFe_{2-x}Nd_xO_4$ nanoparticle catalysts has been determined from the absorption data by using the fundamental relationships.[50,51]

$$I = I_0 e^{\alpha t} \quad (1)$$

$$A = \log(I_0/I) \quad (2)$$

$$\alpha = 2.303(A/t) \quad (3)$$

where, A is the absorption, and t is the thickness of the $NiFe_{2-x}Nd_xO_4$ ferrite samples. To estimate the optical absorption edge for these nanoparticles, $(\alpha h\nu)^{1/n}$ was plotted as a function of the photon energy ($h\nu$) for different n values (n = 1/2, 3/2, 2, 3) (Tauc plots).[52] The best linear fit was obtained in the case of n = 1/2, which indicates a direct allowed optical transition in $NiFe_{2-x}Nd_xO_4$ ferrite nanoparticles. The Tauc plot is presented in Figure 6. The straight line fit to the $(\alpha h\nu)^{1/n}$ vs $h\nu$ plot is obtained by using linear regression software with only very small standard deviation. The intercept of the line at α = 0 gives the value of the optical absorption edge. Figure 6 shows a red shift of absorption edge with Nd substitution into nickel ferrite. Moreover, the extent of red shift increases with the increase in the amount of neodymium substitution like in our previous report.[36] The calculated energy band gap for nickel ferrite was found to be 2.28 eV. This band gap value is nearly equal to experimental values reported in the literature.[29] The sample x = 1.5 shows a large red shift of 1.76

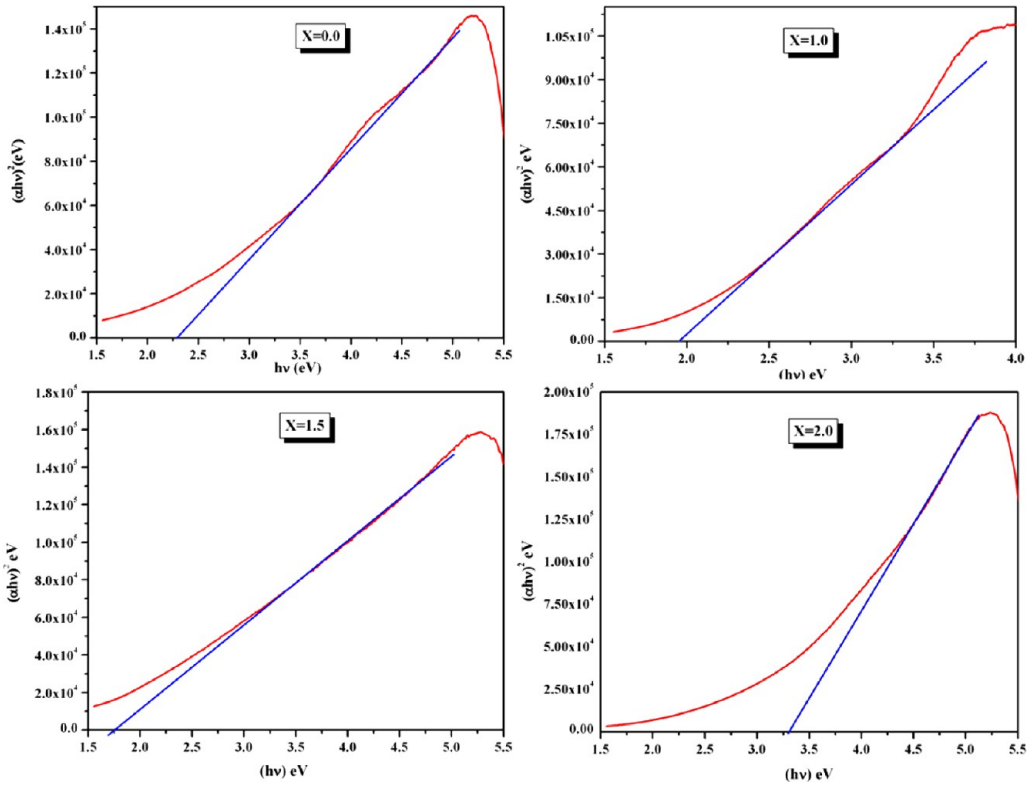

Figure 6. Plot of $(\alpha h\nu)^2$ as a function of photon energy ($h\nu$) for $NiFe_{2-x}Nd_xO_4$ compositions.

eV compared to other samples (for other samples, the x = 1.0 and 2.0 energy band gap was found to be 1.97 and 3.3 eV, respectively). The red shift in energy band gap is considered to be due to two factors in the study. One of these comes from the substitution of neodymium into $NiFe_2O_4$. A partial replacement of Fe^{3+} ions by Nd^{3+} ions causes some electronic states to be introduced into the band gap of $NiFe_2O_4$ by Nd 4f electrons, which are located close to the lower edge of the conduction band to form the new lowest unoccupied molecular orbital. As a result, a series of metastable energy levels are formed within the energy gap, resulting in the red shift of the apparent optical band gap,[53,54] whereas in the sample x = 2.0, octahedral Fe^{3+} cations are completely replaced by the Nd^{3+} ions. As a result, the absorption edge transition can be from O-2p to Nd-4f instead of Fe-3d as in pure $NiFe_2O_4$. The Nd−O bond length becomes smaller than that in the normal spinel structure using atomic pair distribution functions.[55] Therefore, in sample x = 2.0, the distance between O-2p and Nd-4f is large, corresponding to a wide energy band gap.

The other factor is considered to be high doping densities that cause the band gap to shrink. This effect is explained by the fact that the wave functions of the electrons bound to the impurity atoms start to overlap as the density of the impurities increase. This overlap forces the energies to form an energy band rather than a discrete level. If the impurity level is shallow, this impurity band reduces the energy band of the host material.[56] The band gap energies of $NiFe_{2-x}Nd_xO_4$ are greater than the theoretical energy required for water splitting (λ > 1.23 eV),[24] and absorption covers the whole visible region due to the introduction of neodymium, indicating that $NiFe_{2-x}Nd_xO_4$ materials can be used as efficient photocatalysts in practical environmental remediation under natural solar light irradiation.

Photocatalytic Activity. The photocatalytic activities of Nd-substituted $NiFe_2O_4$ and pure $NiFe_2O_4$ photocatalysts were evaluated by the degradation of model organic pollutant rose bengal (RB) under natural solar light irradiation. In order to obtain the real photodegradation yield due to the photocatalysis in the presence of photocatalysts, the decreases in the dye concentration because of the adsorption and direct photolysis should be deducted. The decrease due to adsorption can be deducted after the adsorption equilibrium was achieved. Therefore, photodegradation yield is defined as[57]

$$\text{photodegradation yield} = \frac{C_o - C_a - C_b}{C_o} \times 100$$

where C_o is the initial concentration of the dye, C_a is the concentration after photodegradation of the dye, and C_b is the decrease in concentration because of direct photolysis. Figure 7(a) illustrates the photodegradation rates of rose bengal (RB) on the as-obtained $NiFe_{2-x}Nd_xO_4$ nanocomposite photocatalysts with differing neodymium content under natural solar light irradiation at different time intervals. Blank experiments indicate that the direct photolysis of RB is negligible when illuminated with solar light in the absence of catalysts. The adsorption−desorption equilibrium solutions of RB and $NiFe_{2-x}Nd_xO_4$ were used as starting solutions (t = 0 min). It was observed that compared to other samples pure $NiFe_2O_4$ and $NiNd_2O_4$ nanoparticles are photocatalytically inert compounds (Figure 7(a), [A] and [D]). Interestingly, the neodymium-substituted nickel ferrite hybrid leads to dramatic enhancement of photocatalytic activity (Figure 7(a), [B] and [C]). With increasing neodymium content in the $NiFe_{2-x}Nd_xO_4$ photocatalyst, faster RB degradation was observed, and the neodymium concentration at x = 1.5 gave the best performance in photocatalytic activity (Figure 7(a), [C]). It can

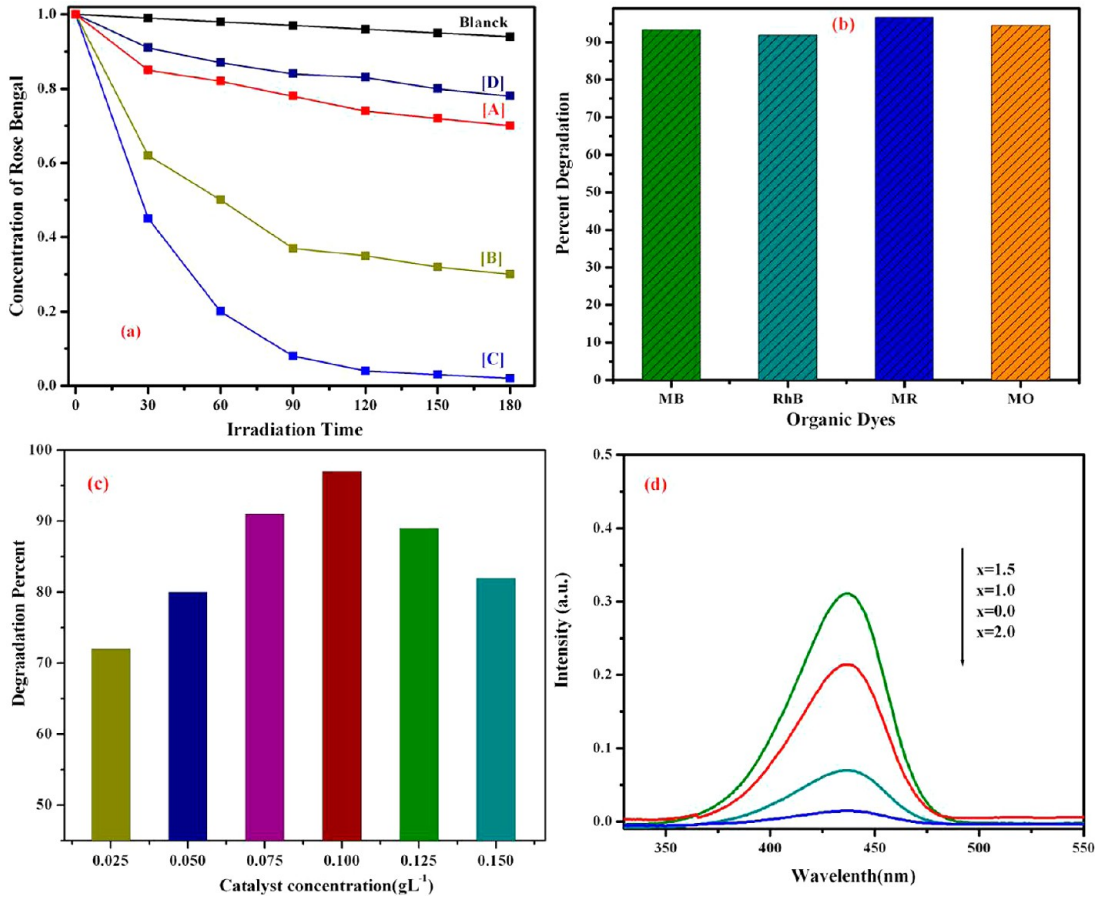

Figure 7. (a) Degradation of rose bengal (10.0 mg L^{-1}) with different $NiFe_{2-x}Nd_xO_4$ photocatalysts under solar light irradiation: [A] x = 0.0, [B] x = 1.0, [C] x = 1.5, [D] x = 2.0. (b) Comparison of percent degradation of different dyes (10.0 mg L^{-1}) with sample x = 1.5. (c) Influence of catalyst concentration on the degradation of rose bengal. (d) Photoluminescence emission spectra of $NiFe_{2-x}Nd_xO_4$ nanoparticles.

be clearly seen that almost all the RB molecules in the solution were decomposed near 180 min for the sample x = 1.5 under natural solar light irradiation.

The photocatalytic activity increases with an increase in neodymium concentration because of the two reasons discussed in the following sections. The first reason is that the higher efficiency of sample x = 1.5 in comparison with other samples (x = 0.0, 1.0, 2.0) can be correlated to its ability to absorb a larger fraction of visible light,[36] as demonstrated in Figure 5. Whereas in comparison with other samples, x = 1.0 ($NiFe_2O_4$) and x = 2.0 ($NiNd_2O_4$) show little absorption in the visible light region due to the large energy band gap (2.29 and 3.3 eV, respectively). Considering the other ferrite samples, the sample at x = 1.5 has a narrow band gap energy (1.76 eV) due to a new energy level appearing at just below the conduction band, which is mainly derived from the electronic states of the introduced neodymium ion (i.e., energy level of introduced neodymium). The significant enhancement in photoactivity with neodymium can be attributed to the substitution effect of the combination of $NiFe_2O_4$ and the neodymium content, leading to the efficient separation of photogenerated carriers in the $NiFe_{2-x}Nd_xO_4$ coupling system. Once it reaches a limit value (such as x = 1.5), the activity decreases (as shown in Figure 7 (a)), possibly because the surface species may also act as recombination centers for charge carriers and also due to a wide band gap.

The second reason is that the substitution of Fe^{3+} by Nd^{3+} in the lattice of $NiFe_2O_4$ is very interesting. The highest photocatalytic activity was shown by the Nd- substituted nickel ferrites ($NiFe_{2-x}Nd_xO_4$). It seems that the octahedrically coordinated Nd^{3+} ions have an important contribution to the formation of new types of defects that are beneficial for photodegradation process. The substitution of Fe^{3+} with isoelectric Nd^{3+} does not create electrically charged lattice defects. However, on the other hand, the replacement of small Fe^{3+} (0.78 Å) with the significantly larger Nd^{3+} (1.16 Å) is likely to induce significant lattice strains. This affects the catalytic activity due to the stabilization of unusual oxidation states and the simultaneous formation of structural defects.[58] Moreover,a narrowed energy band gap can effectively reduce the recombination of photogenerated charge carriers and enhance photocatalytic activity.[59] The photogenerated electrons from the new conduction band due to Nd substitution get transferred to trapping sites of $NiFe_2O_4$ in the presence of sunlight irradiation. Such subsequent transfer of electrons to lattice trapping sites of $NiFe_2O_4$ helps in separating the charge carriers effectively. These trapping sites also benefit by preventing recombination to a large extent and facilitating charge separation thereby activating the catalyst.[60] These factors contribute to improved photocatalytic activity.

The success in synthesis of solar light active $NiFe_{2-x}Nd_xO_4$ by the coprecipitation method and its unusual photocatalytic behavior encouraged us to extend this photocatalytic activity under natural solar light irradiation to another few organic pollutants. Figure 7(b) shows the photodegradation rates of methylene blue (MB), rhodamine B (RhB), methyl orange

dx.doi.org/10.1021/sc400060z | ACS Sustainable Chem. Eng. 2013, 1, 1143−1153

(MO), and methyl red (MR) under the same conditions as for RB. The comparison of their photodegradation yields for the degradation of sample $x = 1.5$ is summarized in Table 2. It was

Table 2. Summary of Photodegradation Yields for Degradation of Different Dyes with Sample $x = 1.5$ under Natural Solar Light Irradiation

Name	Molecular structure	Irradiation light	Photodegradation yield (%)
Rose Bengal (RB)	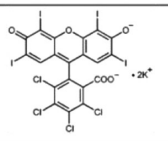	Solar	98.1
Methylene Blue (MB)	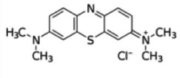	Solar	93.4
Rhodamine B (RhB)	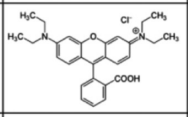	Solar	91.9
Methyl Red (MR)	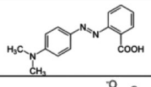	Solar	96.7
Methyl Orange (MO)	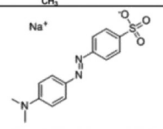	Solar	94.5

observed that the photodegradation yield of these dyes exhibited similar results with a small percent of variation and indicated the effectiveness of the Nd-substituted nickel ferrite ($x = 1.5$). The small percent of variation in the photodegradation yield may depend on the structure and complexity of the dyes, particularly on the nature and position of substituents in the aromatic rings.[61] These results suggest that $NiFe_{2-x}Nd_xO_4$ catalyst can be used to decompose different types of organic pollutants that are present in water.

Effect of Catalyst Concentration. The effect of photocatalyst concentration on the photodegradation of rose bengal (RB) was investigated by employing different concentrations of the sample $x = 1.5$, varying from 0.025 to 0.15g L^{-1}, is as shown in Figure 7(c). This revels that the photodegradation percent of the model compound under investigation was found to increase with the increase in catalyst concentration. As the catalyst amount continues to be increased up to 0.1 g, the degradation increases to 95%. This indicates that a higher catalyst dosage causes an elevated reaction rate because the increase in catalyst amount provides more active sites for RB, leading to a increase in the $OH^{\bullet}$ radical responsible for the degradation of RB. At lower catalyst loading, much of light may be transmitted through the solution, which restricts the catalytic activity. However, when the catalyst amount exceeds 0.1 g, the degradation rate decreases due to the scattering of light and reduction in light penetration through the solution.[62,63] On the basis of this, we found that the optimum catalyst loading for the best photodegradation is 0.1g L^{-1}.

Hydroxyl Radical Analysis. To understand the active species involved in the photocatalytic process, hydroxyl radicals ($OH^{\bullet}$) were detected on the surface of photoilluminated $NiFe_{2-x}Nd_xO_4$ nanoparticles by the photoluminescence (PL) technique.[62,64] Figure 7(d) shows the comparison of PL intensity for $NiFe_{2-x}Nd_xO_4$ nanoparticles. Usually, PL intensity was proportional to the amount of $OH^{\bullet}$ radicals produced. It could be easily seen that at a fixed time, the concentration of $OH^{\bullet}$ radicals formed in the order is as follows: $x = 1.75 > x = 1.0 > x = 0.0 > x = 2.0$. This is consistent with the order of photocatalytic activities of these samples, indicating that the greater the formation rate of $OH^{\bullet}$ radicals, the higher the photocatalytic activity achieved. Moreover, the above results also show that the $OH^{\bullet}$ radicals are the main active species in the photochemical process of the organic dyes/$NiFe_{2-x}Nd_xO_4$ system.

Photocatalytic Mechanism. On the basis of the above discussions and the literature reports,[64−66] a possible mechanism of photodegradation over $NiFe_{2-x}Nd_xO_4$ nanoparticles can be proposed. As shown in Scheme 1, comparison

Scheme 1. Possible Mechanism of the Photocatalytic Degradation of Organic Pollutants Over $NiFe_{2-x}Nd_xO_4$ Photocatalysts under Natural Solar Light Irradiation

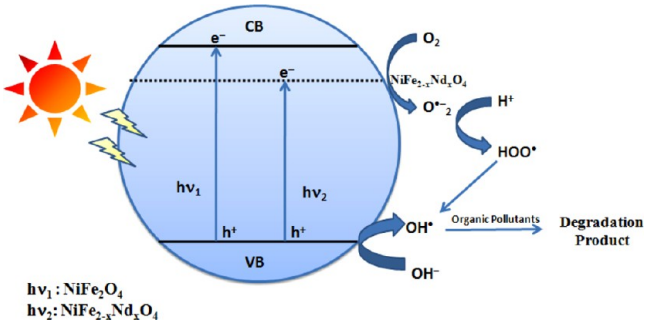

with Nd-substituted $NiFe_2O_4$, pure $NiFe_2O_4$ can hardly be excited by visible light due to its large bandgap (2.28 eV), which leads to a low visible light activity for the photodegradation of organic pollutants. The modification of nickel ferrite by neodymium substitution results in high visible light activity due to a reduction in the band gap. The band gap reduction might be due to the formation of metastable energy levels within the band gap of $NiFe_2O_4$ by Nd 4f electrons, which are located close to the lower edge of the conduction band. Under visible light irradiation, electrons can be excited from the valence band to the energy levels of the $NiFe_{2-x}Nd_xO_4$ system (conduction band) as shown in Scheme 1, and simultaneously the same amount of holes are generated in the VB. Meanwhile, it is highly possible for the photogenerated electrons in the conduction band of nickel ferrite to fall into the energy levels of the $NiFe_{2-x}Nd_xO_4$ system. As a result, the photogenerated electrons and holes can be separated efficiently.[67]

The photoinduced holes directly react with organic dyes or interact with surface-bound H_2O or OH^- to produce the $OH^{\bullet}$ radical species that are extremely strong oxidant for the mineralization of organic dyes. Meanwhile, the electrons that are formed can react with the adsorbed molecular oxygen to yield $O^{\bullet}_2^-$. The generated $O^{\bullet}_2^-$ then further combine with H^+ to produce $HO^{\bullet}_2$,[68] which can react with the trapped electrons to generate $OH^{\bullet}$ radicals.[69] All the reactive species, such as $OH^{\bullet}$, $HO^{\bullet}_2$, $O^{\bullet}_2^-$, and holes, could oxidize organic pollutants to some degree. On the basis of the above analysis, the photocatalytic reaction can be expressed as follows

dx.doi.org/10.1021/sc400060z | ACS Sustainable Chem. Eng. 2013, 1, 1143−1153

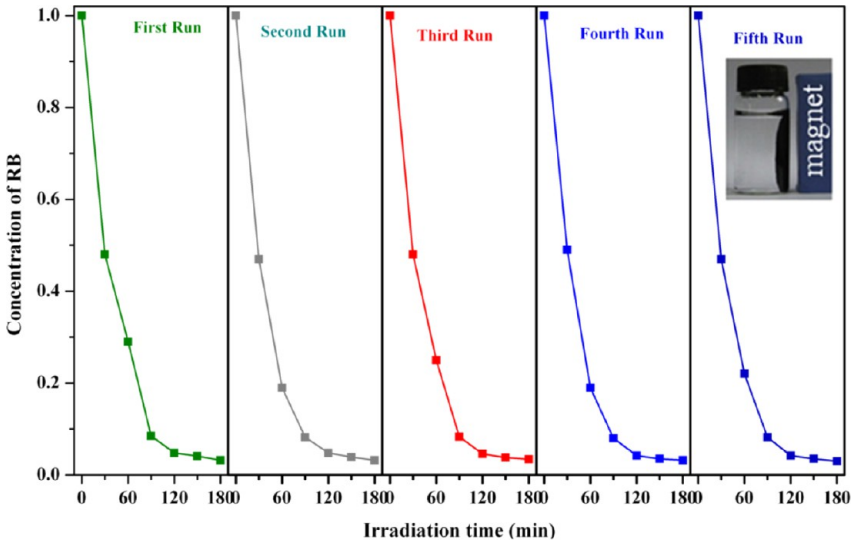

Figure 8. Photodegradation rate of RB in solution for five cycles using $NiFe_{2-x}Nd_xO_4$ (sample $x = 1.5$) photocatalyst under solar light irradiation. Inset reveals the magnetic separation property of $NiFe_{2-x}Nd_xO_4$ nanoparticle catalysts.

$$NiFe_{2-x}Nd_xO_4 + h\nu \rightarrow NiFe_{2-x}Nd_xO_4(e^-_{cb} + h^+_{vb}) \rightarrow NiFe_{2-x}Nd_xO_4 + \text{energy} \quad (4)$$

$$NiFe_{2-x}Nd_xO_4(h^+_{vb}) + H_2O \rightarrow H^+ + OH^\bullet \quad (5)$$

$$NiFe_{2-x}Nd_xO_4(h^+_{vb}) + OH^- \rightarrow OH^\bullet \quad (6)$$

$$NiFe_{2-x}Nd_xO_4(e^-_{cb} + O_2 \rightarrow O^\bullet{}_2^- \quad (7)$$

$$O^\bullet{}_2^- + H^+ \rightarrow HO^\bullet{}_2 \quad (8)$$

$$2e^-_{cb} + HO^\bullet{}_2 + H^+ \rightarrow OH^\bullet + OH^- \quad (9)$$

$$OH^\bullet, HO^\bullet{}_2, O^\bullet{}_2^-, h^+_{vb} + \text{organic pollutants} \rightarrow \text{degradation product} \quad (10)$$

Recycle Ability. The regeneration of the photocatalyst was one of the key steps in the photocatalysis technology for practical applications. $NiFe_2O_4$ is a soft magnetic material that possesses good magnetic properties, which gives it good performance in magnetic separation for the $NiFe_{2-x}Nd_xO_4$ photocatalysts using an external magnet (Figure 8, inset). Herein, the stability of the sample $x = 1.5$ was investigated, and this catalyst can be reused without considerable amount of mass loss. As shown in Figure 8 during the usage of five cycles, the photocatalytic activity was almost as high as the first cycle. These results illustrated that $NiFe_{2-x}Nd_xO_4$ as a novel magnetically separable, highly solar light response photocatalyst and also can be reused for several times efficiently. It exhibits potential application in continual and long-term processes.

CONCLUSION

In summary, for the first time, we have reported that the neodymium-substituted nickel ferrite system could be a promising material for photocatalysis under natural solar light irradiation. The neodymium substitution into nickel ferrite results in a dramatic conversion of the inert $NiFe_2O_4$ into a highly solar light active photocatalyst. This may be due to the reduction of the nickel ferrite band gap by Nd^{3+} substitution. It should be pointed out that the $NiFe_{2-x}Nd_xO_4$ photocatalysts are cost saving, magnetically recoverable, recyclable photocatalysts that exhibit high photocatalytic efficiency (up to 98%) to decompose different types of organic pollutants. In an attempt to design the efficient solar light active photocatalyst, we were successful in optimizing the concentration of Nd^{3+} substitution, large visible light absorption, and energy band gap of the materials. On the basis of experimental results, the strategy for future improvement in the photocatalytic properties of ferrites under solar light irradiation should take into consideration the finding of suitable substitutional elements for Fe^{3+}. This could open new uses for substituted ferrites in applications such as larger scale wastewater treatment plants.

AUTHOR INFORMATION

Corresponding Author

*E-mail: hsb_naik@rediffmail.com. Fax: +91-8282-256255.

Notes

The authors declare no competing financial interest.

ACKNOWLEDGMENTS

K. N. Harish thanks Kuvempu University for providing a junior research fellowship and St. Joseph College, Bangalore, for providing XRD and FTIR spectral data.

REFERENCES

(1) Al-Ghouti, M. A.; Khraisheh, M. A.; Allen, S. J.; Ahmad, M. N. The removal of dyes from textile wastewater: a study of the physical characteristics and adsorption mechanisms of diatomaceous earth. *J. Environ. Manage.* **2003**, *69*, 229−238.

(2) Singh, H. K.; Saquib, M.; Haque, M. M; Muneer, M. Heterogeneous photocatalysed degradation of 4-chlorophenoxyacetic acid in aqueous suspensions. *J. Hazard. Mater.* **2007**, *142*, 374−380.

(3) Su, Y.; Deng, L.; Zhang, N.; Wang, X.; Zhu., X. Photocatalytic degradation of C.I. Acid Blue 80 in aqueous suspensions of titanium dioxide under sunlight. *React. Kinet. Catal. Lett.* **2009**, *98*, 227−240.

(4) Neppolian, B.; Choi, H. C.; Sakthivel, S.; Arabindoo, B.; Murugesan, V. Solar/UV-induced photocatalytic degradation of three commercial textile dyes. *J. Hazard. Mater.* **2002**, *89*, 303−317.

(5) Kuo, W. S.; Ho, P. H. Solar photocatalytic decolorization of methylene blue in water. *Chemosphere* **2001**, *45*, 77−83.

(6) Lewis, N. S.; Nocera, D. G. Powering the planet: Chemical challenges in solar energy utilization. *Proc. Natl. Acad. Sci. U.S.A.* **2007**, *104*, 20142−52.
(7) Alexander, B. D.; Kulesza, P. J.; Rutkowska, L.; Solarska, R.; Augustynski, J. Metal oxide photoanodes for solar hydrogen production. *J. Mater. Chem.* **2008**, *18*, 2298−303.
(8) Kudo, A.; Miseki, Y. Heterogeneous photocatalyst materials for water splitting. *Chem. Soc. Rev.* **2009**, *38*, 253−78.
(9) Liu, G.; Wang, L. Z.; Yang, H. G.; Cheng, H. M.; Lu, G. Q. Titania-based photocatalysts-crystal growth, doping and heterostructuring. *J. Mater. Chem.* **2010**, *20*, 831−43.
(10) Kudo, A. Recent progress in the development of visible light driven powdered photocatalysts for water splitting. *Int. J. Hydrogen Energy* **2007**, *32*, 2673−2678.
(11) Fox, M. A; Dulay, M. T. Heterogeneous photocatalysis. *Chem. Rev.* **1993**, *93*, 341−357.
(12) Mitoraj, D.; Kisch, H. The nature of nitrogen-modified titanium dioxide photocatalysts active in visible light. *Angew. Chem., Int. Ed. Engl.* **2008**, *47*, 9975−9978.
(13) Xu., X.; Liu, G.; Randorn, C.; Irvine, J. T. S. g-C_3N_4 coated $SrTiO_3$ as an efficient photocatalyst for H_2 production in aqueous solution under visible light irradiation. *Int. J. Hydrogen Energy* **2011**, *36*, 13501−13507.
(14) Fu., Y.; Chen, Q.; He., M.; Wan, Y.; Sun, X.; Xia, H.; Wang., X. A multifunctional heteroarchitecture for photocatalysis and energy storage. *Ind. Eng. Chem. Res.* **2012**, *51*, 11700−11709.
(15) Shu, X.; He, J.; Chen, D. Visible-light-induced photocatalyst based on nickel titanate nanoparticles. *Ind. Eng. Chem. Res.* **2008**, *47*, 4750−4753.
(16) Guo, R. Q; Fang, L. A.; Dong, W.; Zheng, F. G.; Shen, M. R. Enhanced photocatalytic activity and ferromagnetism in Gd doped BiFeO3 nanoparticles. *J. Phys. Chem. C* **2010**, *114*, 21390−21396.
(17) Shylesh, S.; Schunemann, V.; Thiel, W. R. Magnetically separable nanocatalysts: Bridges between homogeneous and heterogeneous catalysis. *Angew. Chem., Int. Ed.* **2010**, *49*, 3428−3459.
(18) Borse, P. H.; Hwichan, J.; Choi, S. H.; Hong, S. J.; Lee, J. S. Phase and photoelectrochemical behavior of solution-processed Fe_2O_3 nanocrystals for oxidation of water under solar light. *Appl. Phys. Lett.* **2008**, *93*, 173103−3.
(19) Tamaura, Y.; Ueda, Y.; Matsunami, J.; Hasegawa, N.; Nezuka, M.; Sano, T.; Tsuji, M. Solar hydrogen production by using ferrites. *Sol. Energy* **1999**, *65*, 55−57.
(20) Benko, F. A.; Koffyberg, F. P. The effect of defects on some photoelectrochemical properties of semiconducting $MgFe_2O_4$. *Mater. Res. Bull.* **1986**, *21*, 1183−1188.
(21) Han, S. B.; Kang, T. B.; Joo, O. S.; Jung, K. D. Water splitting for hydrogen production with ferrites. *Sol. Energy* **2007**, *81*, 623−628.
(22) Yu, S. H.; Yoshimura, M. Ferrite/metal composites fabricated by soft solution processing. *Adv. Funct. Mater.* **2002**, *12*, 9−15.
(23) Nan, C.-W.; Bichurin, M. I.; Dong, S.; Viehland, D.; Srinivasan, G. Multiferroic magnetoelectric composites: Historical perspective, status, and future directions. *J. Appl. Phys.* **2008**, *103*, 031101.
(24) Jang, J. S.; Hong, S. J.; Lee, J. S.; Borse, P. H; Kim, H. G. Synthesis of zinc ferrite and its Photocatalytic applications under sun light. *J. Korean Phys. Soc.* **2009**, *54*, 204−208.
(25) Dom, R.; Subasri, R.; Radha, K.; Borse, P. H. Synthesis of solar active nano crystalline ferrite, MFe_2O_4 (M: Ca, Zn, Mg) photocatalyst by microwave irradiation. *Solid State Commun.* **2011**, *151*, 470−473.
(26) Tsoncheva, T.; Manova, E.; Velinov, N.; Paneva, D.; Popova, M.; Kunev, B.; Tenchev, K.; Mitov, I. Thermally synthesized nanosized copper ferrites as catalysts for environment protection. *Catal. Commun.* **2010**, *12*, 105−109.
(27) Su, M.; He, C.; Sharma, V. K.; Asi, M. A.; Xia, D.; Li, X.-z.; Deng, H.; Xiong, Y. Mesoporous zinc ferrite: Synthesis, characterization, and photocatalytic activity with H_2O_2/visible light. *J. Hazard. Mater.* **2012**, *211−212*, 95−103.
(28) Kinemuchi, Y.; Ishizaka, K.; Suematsu, H.; Jiang, W. H.; Yatsui, K. Magnetic properties of nanosize $NiFe_2O_4$ particles synthesized by pulsed wire discharge. *Thin Solid Films* **2002**, *407*, 109−113.
(29) Balaji, S.; Kalaiselvan, R.; Berchmans, L. J.; Angappan, S.; Subramanian, K.; Augustin, C. O. Combustion synthesis and characterization of Sn_4^+ substituted nanocrystalline $NiFe_2O_4$. *Mater Sci Eng* **2005**, *119*, 119−124.
(30) Fu, Y.; Chen, H.; Sun, X.; Wang, X. Graphene-supported nickel ferrite: A magnetically separable photocatalyst with high activity under visible light. *AIChE J.* **2012**, *58*, 3298−3305.
(31) Kundu, T. K.; Mishra, S.; Karak, N.; Barik, P. Effect of Ti^{4+} ions doping on microstructure and dc resistivity of C. *J. Phys. Chem. Solids* **2012**, *73*, 579−583.
(32) Peng, Z.; Fu, X.; Ge, H.; Fu, Z.; Wang, C.; Qi, L.; Miao, H. Effect of Pr^{3+} doping on magnetic and dielectric properties of Ni−Zn ferrites by "one-step synthesis". *J. Magn. Magn. Mater.* **2011**, *323*, 2513−2518.
(33) Xu, S.; Shangguan, W.; Yuan, J.; Chen, M.; Shi, J. Preparation and photocatalytic properties of magnetically searable TiO_2 supported on nickel ferrite. *Chin. J. Chem. Eng.* **2007**, *15* (2), 190−195.
(34) Singh, J. P.; Dixit, G.; Srivastava, R. C.; Agrawal, H. M.; Asokan, K. Looking for the possibility of multiferroism in $NiGd_{0.04}Fe_{1.96}O_4$ nanoparticle system. *J. Phys. D: Appl. Phys.* **2011**, *44*, 435306.
(35) Ishaque, M.; Islam, M. U.; Azhar Khan, M.; Rahman, I. Z.; Genson, A.; Hampshire, S. Structural, electrical and dielectric properties of yttrium substituted nickel ferrites. *Phys. B* **2010**, *405*, 1532−1540.
(36) Harish, K. N.; Bhojya Naik, H. S.; Prashanth kumar, P. N.; Viswanath, R. Synthesis, enhanced optical and photocatalytic study of Cd−Zn ferrites under sunlight. *Catal. Sci. Technol.* **2012**, *2*, 1033−1039.
(37) Maaz, K.; Karim, S.; Mashiatullah, A.; Liu, J.; Hou, M. D; Sun, Y. M; Duan, J. L; Yao, H. J; Mob, D.; Chen, Y. F. Synthesis and magnetic characterization of nickel ferrite nanoparticles prepared by co-precipitation route. *J. Magn. Magn. Mater.* **2009**, *321*, 1838−1842.
(38) Jolivet, J. P.; Chaneac, C.; Prene, P.; Vayssieres, L.; Tronc, E. Wet chemistry of spinel iron oxide particles. *J. Phys. IV France* **1997**, *7*, C1−573.
(39) Zhao, L.; Yang, H.; Yu, L.; Cui, Y.; Zhao, Z.; Feng, S. Magnetic properties of Re-substituted Ni−Mn ferrite nanocrystallites. *J. Mater. Sci.* **2007**, *42*, 686−691.
(40) von Grande, B.; Muller-Buschbaum, H. K; Schweizer, M. *Z. Anorg. Allgem. Chem.* **1975**, *414*, 76.
(41) Shinde, T. J; Gadkari, A. B; Vasambekar, P. N. Influence of Nd^{3+} substitution on structural, electrical and magnetic properties of nanocrystalline nickel ferrites. *J. Alloys Compd.* **2012**, *513*, 80−85.
(42) Vermenko, L. A; Gridasova, T. Y; Lukachina, E. N. *Consultants Bureau*; Division of Plenum Publishing Corporation: New York, 1974; pp 732−735.
(43) Zhu, X. F; Chen, L. F. First-principles study of the electronic and magnetic properties of a nickel−zinc ferrite: $Zn_xNi_{1-x}Fe_2O_4$. *J. Magn. Magn. Mater.* **2011**, *323*, 3138−3142.
(44) Koseog, Y.; Baykal, A.; Gozuak, F.; Kavas, H. Structural and magnetic properties of $Co_xZn_{1-x}Fe_2O_4$ nanocrystals synthesized by microwave method. *Polyhedron* **2009**, *28*, 2887−2892.
(45) Hemeda, O. M; Barakat, M. M; Hemeda, D. M. Structural, electrical and spectral studies on double rare-earth orthoferrites $La_{1-x}Nd_xFeO_3$. *Turk. J. Phys.* **2003**, *27*, 537−549.
(46) Ahmed, M. A; Ateia, E.; El-Dek, S. I. Spectroscopic analysis of ferrite doped with different rare earth elements. *Vib. Spectrosc.* **2002**, *30*, 69−75.
(47) Botta, P. M; Aglietti, E. F; Porto López, J. M. Kinetic study of $ZnFe_2O_4$ formation from mechanochemically activated Zn−Fe_2O_3 mixtures. *Mater. Res. Bull.* **2006**, *41*, 714−723.
(48) Lv, H; Ma, L.; Zeng, P.; Ke, D.; Peng., T. Synthesis of floriated $ZnFe_2O_4$ with porous nanorod structures and its photocatalytic hydrogen production under visible light. *J. Mater. Chem.* **2010**, *20*, 3665−3672.
(49) Nassoko, D.; Li, Y.-F.; Li, J.-L.; Li, X.; Yu, Y. Neodymium-doped TiO_2 with anatase and brookite two phases: Mechanism for photocatalytic activity enhancement under visible light and the role

of electron. *Int. J. Photoenergy* **2012**, DOI: 10.1155/2012/716087, , Article ID 716087..
(50) Pathan, H. M.; Desai, J. D.; Lokhande, C. D. Modified chemical deposition and physico-chemical properties of copper sulphide (Cu_2S) thin films. *Appl. Surf. Sci.* **2002**, *202*, 47−56.
(51) Srivastava, M.; Ojhaa, A. K; Chaubeya, B. S; Maternyb, A. Synthesis and optical characterization of nanocrystalline $NiFe_2O_4$ structures. *J. Alloys Compd.* **2009**, *481*, 515−519.
(52) Tauc, J. *Amorphous and Liquid Semiconductor*; Plenum: New York, 1974. *159*.
(53) Kislov, N.; Srinivasan, S. S; Emirov, Yu; Stefanakos, E. K. Optical absorption red and blue shifts in $ZnFe_2O_4$ nanoparticles. *Mater. Sci. Eng., B* **2008**, *153*, 70−77.
(54) Li, W.; Wang, Y.; Lin, H.; Ismat Shah, S.; Huang, C. P.; et al. Band gap tailoring of Nd^{3+}-doped TiO_2 nanoparticles. *Appl. Phys. Lett.* **2003**, *83*, 20.
(55) Ishimaru, M.; Hirotsu, Y.; Afanasyev-Charkin, I. V; Sickafus, K. E. Atomistic structures of metastable and amorphous phases in ion-irradiated magnesium−aluminate spinel. *J. Phys.: Condens. Matter.* **2002**, *14*, 1237−1247.
(56) van Zeghbroeck B. V. *Principles of Semiconductor Devices and Heterojunctions*; Prentice Hall: Upper Saddle River, NJ, **2011**; 0130409049.
(57) Wu, Y.; Liu, S.; Zuo, Y.; Li, J.; Wang, J. Photodegradation of some dyes over Ce/FSM-16 catalyst under solar light. *Catal. Lett.* **2007**, *119*, 245.
(58) Papa, F.; Patron, L.; Carp, O.; Paraschiv, C.; Ioan, B. Catalytic activity of neodymium substituted zinc ferrites for oxidative conversion of methane. *J. Mol. Catal A: Chem.* **2009**, *299*, 93−97.
(59) Wang, E.; He, T.; Zhao, L.; Chen, Y.; Gao, Y. Improved visible light photocatalytic activity of titania doped with tin and nitrogen. *J. Mater. Chem.* **2010**, *21*, 144−150.
(60) Aziz, A. A.; Yong, K. S.; Ibrahim, S.; Pichiah, S. Enhanced magnetic separation and photocatalytic activity of nitrogen doped titania photocatalyst supported on strontium ferrite. *J. Hazard. Mater.* **2012**, *199− 200*, 143−150.
(61) Chen, K. C; Wua, J. Y; Liou, D. J; Hwang, S. C. J Decolorization of the textile dyes by newly isolated bacterial strains. *J. Biotechnol.* **2003**, *101*, 57.
(62) Li, F.-t.; Zhao, Y.; Liu, Y.; Hao, Y.-j.; Liu, R.-h.; Zhao, D.-s. Solution combustion synthesis and visible light-induced photocatalytic activity of mixed amorphous and crystalline $MgAl_2O_4$ nanopowders. *Chem. Eng. J.* **2011**, *173*, 750−759.
(63) Gonçalves, M. S. T; Oliveira-Campos, A. M. F.; Pinto, E. M. M. S; Plasencia, P. M. S.; Queiroz, M. J. R. P. Photochemical treatment of solutions of azo dyes containing TiO_2. *Chemosphere* **1999**, *39*, 781−786.
(64) Li, X.; Hou, Y.; Zhao, Q.; Wang, L. A general, one-step and template-free synthesis of sphere-like zinc ferrite nanostructures with enhanced photocatalytic activity for dye degradation. *J. Colloid Interface Sci.* **2011**, *358*, 102−108.
(65) Horikoshi, S.; Saitou, A.; Hidaka, H.; Serpone, N. Environmental remediation by an integrated microwave/UV illumination method. V. Thermal and nonthermal effects of microwave radiation on the photocatalyst and on the photodegradation of rhodamine-B under UV/vis radiation. *Environ. Sci. Technol.* **2003**, *37*, 5813.
(66) Chen, Z. X; Li, D. Z; Zhang, W. J; Shao, Y.; Chen, T. W; Sun, M.; Fu, X. Z Photocatalytic degradation of dyes by $ZnIn_2S_4$ microspheres under visible light irradiation. *J. Phys. Chem. C* **2009**, *113*, 4433.
(67) Wang, E.; Zhang, P.; Chen, Y.; Liu, Z.; He, T.; Cao, Y. Improved visible-light photocatalytic activity of titania activated by nitrogen and indium modification. *J. Mater. Chem.* **2012**, *22*, 14443−14449.
(68) Horikoski, S.; Tokunaga, A.; Hidaka, H.; Serpone, N. Environmental remediation by an integrated microwave/UV illumination method: VII. Thermal/non-thermal effects in the microwave-assisted photocatalyzed mineralization of bisphenol-A. *J. Photochem. Photobiol., A* **2004**, *162*, 33.
(69) Kaneco, S.; Rahman, M. A; Suzuki, T.; Katsumata, H.; Ohta, K. Optimization of solar photocatalytic degradation conditions of bisphenol A in water using titanium dioxide. *J. Photochem. Photobiol., A.* **2004**, *163*, 419.